Journal of Materials Science: Materials in Electronics (2019) 30:17963–17971
https://doi.org/10.1007/s10854-019-02150-x

Effect of dispersion on visible light transmittance and resistivity of indium tin oxide nanoparticles prepared by cetyltrimethylammonium bromide-assisted coprecipitation method

Yunqian Ma[1] · Fei Liang[2] · Youxing Liu[3] · Xiaoyu Zhai[1] · Jiaxiang Liu[1]

Received: 26 July 2019 / Accepted: 3 September 2019 / Published online: 10 September 2019

Abstract

A new strategy for decreasing resistivity while increasing visible light transmission of indium tin oxide nanoparticles (ITO NPs) was reported in this paper. Cubic phase ITO NPs with high dispersion were synthesized by coprecipitation method with cetyltrimethylammonium bromide (CTAB) assisted. The effects of dispersion on the optical and electrical properties of ITO NPs were investigated systematically. Surface potential of ITO NPs synthesized with 1.5 g/L of CTAB was increased from −4.5 to 13.0 mV, resulting in an increase in visible light transmittance of ITO NPs from 70 to 92% and a decrease in resistivity from 6.5×10^{-1} to 3.5×10^{-1} Ω cm. The fitting equation between the visible light transmittance (T) of ITO NP and its absolute value of Zeta potential (μ) was $T = 60.862 + 2.287\mu$, while the fitting equation of its resistivity (ρ) and absolute value of Zeta potential (μ) was $\rho = 0.7968 - 0.0350\mu$. This result showed that the dispersion of ITO NPs had a great contribution to improving their optical and electrical properties. And the mechanism of the influence of dispersion on optical and electrical properties of ITO NPs was also discussed.

1 Introduction

Indium tin oxide (ITO) films, as transparent conductive oxides [1, 2], have caused much attention of domestic and foreign scholars on account of their excellent physical and chemical properties, such as high electrical conductivity, high visible light transmittance, high work function, high infrared light reflection and strong ultraviolet (UV) absorption [3–6]. ITO films are mainly used in the fields of solar cells [7], light-emitting diodes [8] and sensors [9, 10]. There are a lot of methods for fabricating ITO films, including ion-beam sputtering [11], spray pyrolysis [12], electron beam evaporation [13] and chemical vapor deposition (CVD) [14, 15]. ITO nanoparticle with high performance is indispensable for preparation ITO films of high quality by these above methods. Therefore, ITO NPs with low resistivity used as important raw materials for the preparation of ITO films with high performance were wildly investigated [16, 17]. In order to fabricate ITO films with high visible light transmittance and conductivity, a series of factors, including atomic doping ratio of Sn and In, temperature and structure of ITO have already been explored [18, 19]. However, the visible light transmittance properties of ITO NPs have not received much attention yet. As we all know, the performance of ITO films is affected by the properties of ITO NPs. Therefore, it is of great significance to investigate the visible light transmittance of ITO NPs.

Many methods have been explored to prepare nanoparticles with good properties [20–24]. As one of facile methods for preparing nanopowders, chemical coprecipitation method with simple equipment and low cost is commonly used to synthesize ITO NPs [25, 26]. However, the disadvantage of chemical coprecipitation method is that the as-prepared nanoparticles have a poor dispersion, which may inhibit the performance of ITO NPs, including resistivity and visible

✉ Jiaxiang Liu
ljxpost@263.net

1 The Beijing Key Laboratory of Electrochemical Process and Technology for Materials, Beijing University of Chemical Technology, Beijing 100029, People's Republic of China

2 National Center for Nanoscience and Technology, Beijing 100190, People's Republic of China

3 Institute of Chemistry Chinese Academy of Sciences, Beijing 100190, People's Republic of China

light transmission. Therefore, it is necessary to synthesize ITO NPs with high dispersibility to further increase their performance through a facile coprecipitation method.

Both optical and electrical properties are important for ITO as a transparent conductive oxide material. In this paper, we have innovatively designed an ingenious route to improve the dispersion of ITO NPs synthesized through chemical coprecipitation method, which not only increased the visible light transmittance of ITO NPs, but also reduced their resistivity. CTAB as an excellent dispersant was used to improve the dispersion of ITO NPs. And the schematic illustration of the experimental process is shown in Fig. 1. The effect of dispersion of ITO NPs on their optical and electrical properties was investigated systematically. In addition, the equations established based on the dispersion of ITO NPs in our paper can be used to estimate their optical and electrical properties, which will provide scholars with theoretical basis and guiding significance about the effect of dispersibility on the performance of the powders.

2 Experiment

Metal indium (purity > 99.99%) was purchased from Liuzhou Smelting Co. Ltd. $SnCl_4 \cdot 5H_2O$ (purity > 99.99%) was purchased from Sinopharm Chemical Reagent Co. Ltd. Ammonia was purchased from Beijing Chemical Factory. Cetyltrimethylammonium bromide (CTAB) was purchased from Bailingwei Technology Co. Ltd. All reagents were not further purified.

22.8 g of metal indium was dissolved into concentrated nitric acid (HNO_3) at 50 °C (Solution A), and then 7.01 g of $SnCl_4 \cdot 5H_2O$ was dissolved into deionized water (Solution B). The mixed solution was obtained by mixing the above two solutions (Solution A and B). CTAB with different concentrations was added to the mixed solution, including 0.0, 0.5, 1.0, 1.5 and 2.0 g/L. Ammonia was used as precipitant and pH regulator to adjust the pH to 9, stirring for 2 h. The precipitate was washed with DI water and ethanol for several times, respectively, until the ions of chlorine and nitrate were removed completely. And then, indium tin hydroxide, the precursor, was dried at 30 °C for 10 h. ITO NP was obtained by calcining the precursor in a muffle furnace at 600 °C for 4 h.

The crystal structure of $In(OH)_3$ NPs and ITO NPs was studied by X-ray powder diffraction (XRD, D8 Advance). X-ray Photoelectron Spectroscopy (XPS, ESCALAB 250) and Fourier transform infrared spectrometer (FT-IR, NICOLTE 6700) were used to study the characteristic of chemical bond of $In(OH)_3$ NPs and ITO NPs. The dispersion and particle size of ITO powders were investigated by Zeta potentiometer (Zeta PALS) and scanning electron microscope (SEM, HITACHI S-4700) respectively. The light performance and electrical performance of ITO NPs were tested by UV–visible spectrophotometer (UV-3600) and four-probe resistance meter (SZ-82) respectively.

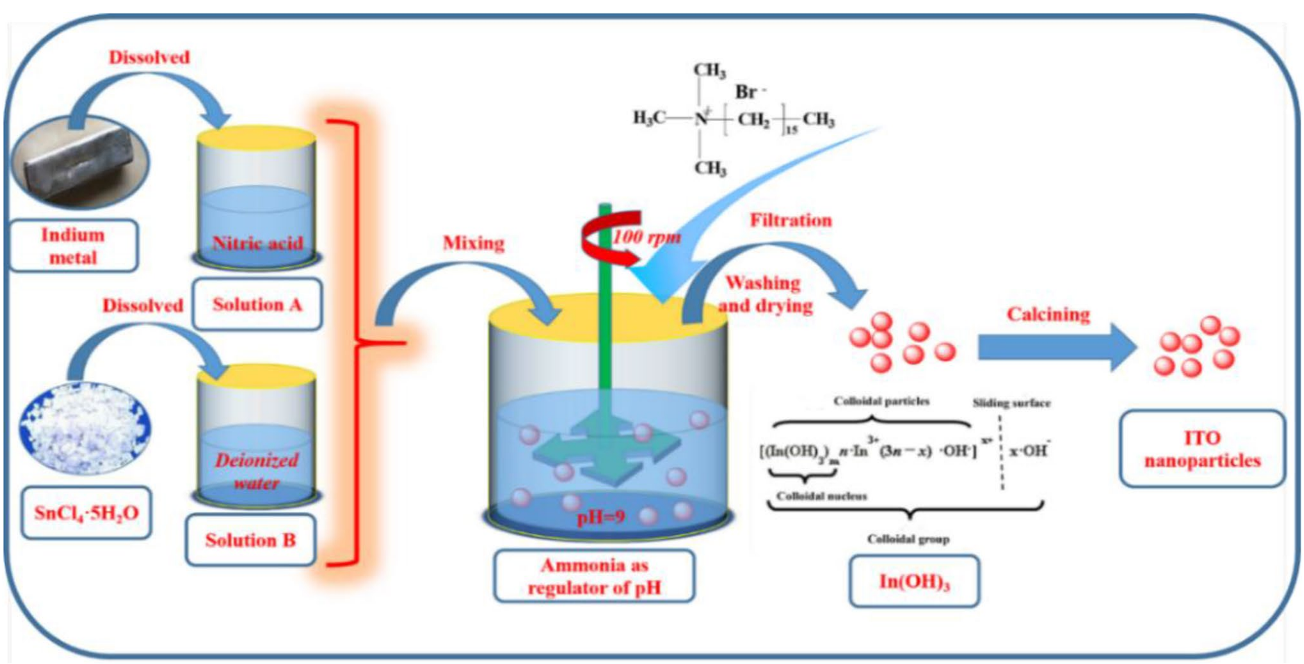

Fig. 1 Schematic illustration of the experimental process

3 Results and discussion

3.1 The phase characterization of ITO NPs

The synthesis conditions may have an influence on the growth and crystal phase of nanoparticles [27–31]. In order to explore the crystal phase and formation process of ITO NPs synthesized with different concentrations of CTAB, the tests of XRD and FT-IR were carried out. The XRD pattern of the precursors and final products prepared with different concentrations of CTAB are shown in Fig. 2. As can be seen from Fig. 2a, the diffraction peaks of all the precursors can be indexed to the same crystal phase of $In(OH)_3$, and there are no other impurity phases, indicating that CTAB as a dispersant adsorbed on the surface of $In(OH)_3$ did not change the crystal structure of $In(OH)_3$ NPs. Cubic phase ITO NPs were obtained after calcination of $In(OH)_3$, the XRD patterns are shown in Fig. 2b and the sharp diffraction peaks indicate high crystallinity.

The formation mechanism of ITO NPs can be explained by Eqs. (1) and (2). Ammonia was used as precipitant and pH regulator in this work, and then the precursor, $In(OH)_3$, was obtained in alkaline conditions (Eq. 1), which can be proved by the XRD pattern shown in Fig. 2a. ITO NPs were finally prepared by dehydrating of $In(OH)_3$ in a muffle furnace at 600 °C for 4 h (Eq. 2).

$$In^{3+} + 3OH^- \xrightarrow{pH=9} In\,(OH)_3 \tag{1}$$

$$2In(OH)_3 \xrightarrow{Calcining} In_2O_3 + 3H_2O \tag{2}$$

The FT-IR spectra of $In(OH)_3$ synthesized with different concentrations of CTAB is shown in Fig. 3, there are many characteristic absorption peaks. The absorption peaks at 500 cm^{-1} and 3235 cm^{-1} can be attributed to the stretching vibrations of In-OH and O–H, respectively. The absorption peaks at 1385 cm^{-1} and 1616 cm^{-1} represent the stretching vibrations of C–C and C–N, indicating the adsorption of CTAB on $In(OH)_3$ surface. The absorption peak at 3380 cm^{-1} corresponds to the stretching vibration of O–H of H_2O [32]. Two new absorption peaks appear at 603 cm^{-1} and 568 cm^{-1} on account of the formation of ITO NPs after calcination [33]. Additionally, the XRD pattern of the precursors (Fig. 2a) confirms the formation of $In(OH)_3$, while the O_{1s} XPS spectra of the final products proves the formation of ITO NPs (Fig. 3b).

3.2 The effects of CTAB on the dispersion of ITO NPs

As we all know, the dispersion of powders is closely related to their Zeta potential. The higher the absolute value of Zeta potential, the greater the electrostatic repulsion among the nanoparticles, and the better their dispersion. In other words, the dispersion of NPs increases significantly with the increase of their absolute value of Zeta potential. The surface repulsion energy (Φ) among the particles can be calculated via Eq. (3) according to DLVO theory [34].

$$\Phi = \frac{64 n_0 k T \gamma_0^2}{\delta} \exp(-\delta d) \tag{3}$$

Wherein, n_0 represents the particle concentration, k is Boltzmann constant, T is absolute temperature, d is the distance between particles, δ represents the reciprocal of the thickness of the double layer, γ_0 can be explained via Eq. (4).

$$\gamma_0 = \frac{\exp\left(\frac{ze\Psi_0}{2kT}\right) - 1}{\exp\left(\frac{ze\Psi_0}{2kT}\right) + 1} \tag{4}$$

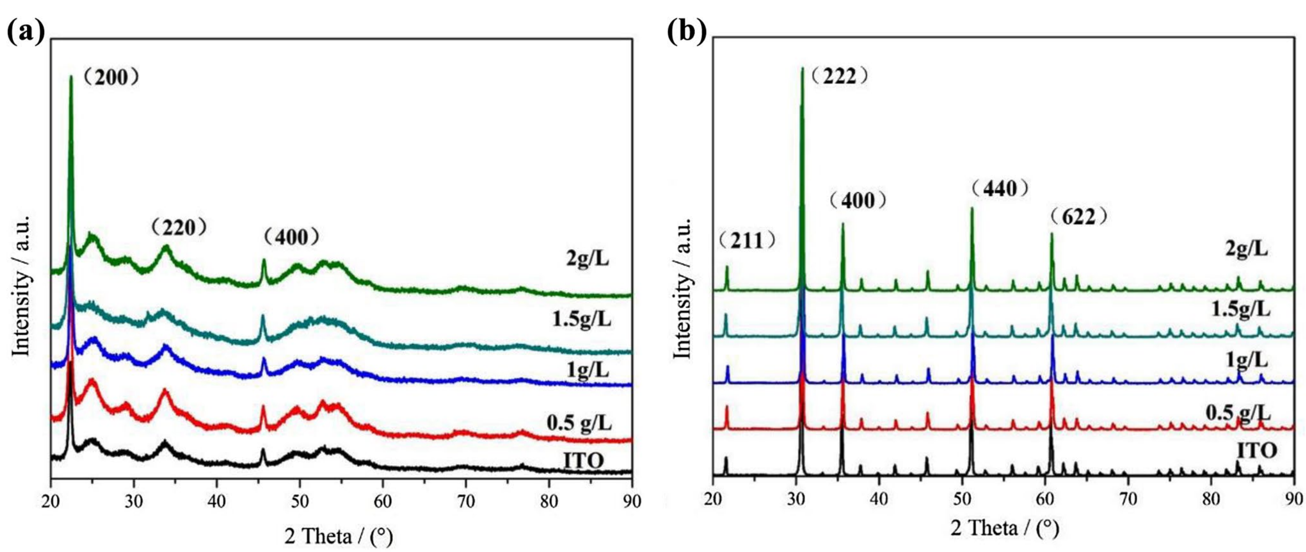

Fig. 2 XRD pattern of **a** $In(OH)_3$ and **b** ITO NPs prepared with different concentrations of CTAB

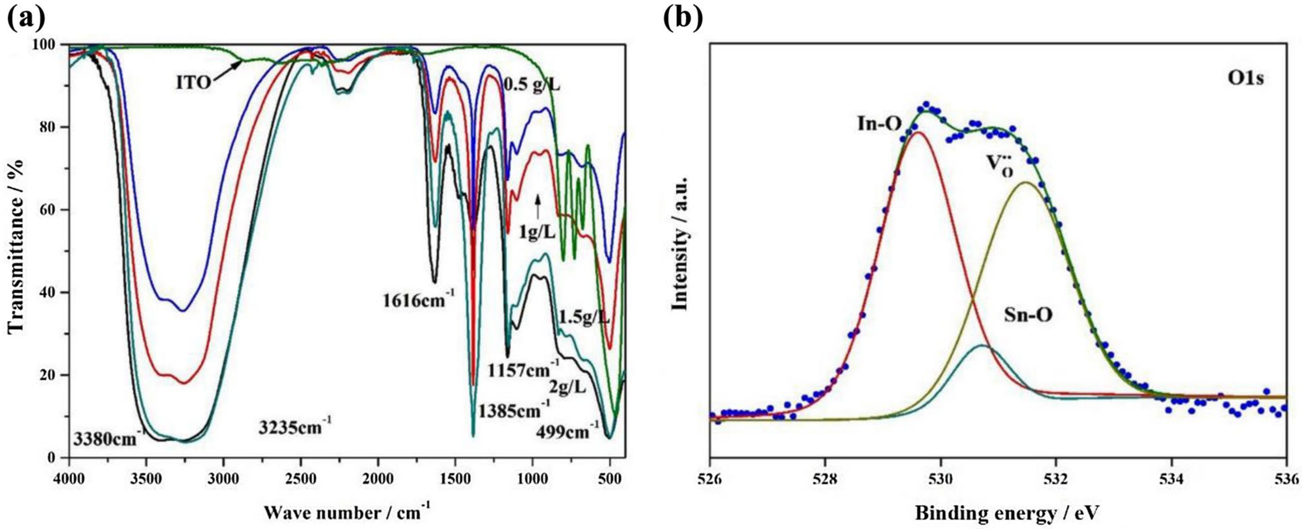

Fig. 3 **a** FT-IR spectra of $In(OH)_3$ prepared with different concentrations of CTAB and **b** O_{1s} XPS spectra of ITO nanoparticles

In this equation, *ze* is the electric quantity of particles, Ψ_0 is the surface potential. Therefore, the dispersion of powders can be improved by increasing the absolute value of surface potential measured via Zeta potentiometer. The higher the absolute value of surface potential, the better the dispersion of nanoparticles.

In order to select the appropriate pH value, the Zeta potential of the precursors at different pH values were tested, shown in Fig. 4. It can be seen that the Zeta potential keeps decreasing as the pH value increases from 2 to 9. In addition, the isoelectric point (IEP) can be reached at the pH value of about 8, indicating that the colloidal particles of $In(OH)_3$ are negatively charged when pH value is greater than 8, which is conducive to the adsorption of CTAB as a cationic surfactant on the surface of $In(OH)_3$ NPs. Therefore, the pH of 9 is chosen as the optimal condition to obtain the precipitation of indium tin hydroxide.

When the pH value of the solution is 9, the $In(OH)_3$ colloid is negatively charged. The structure of $In(OH)_3$ colloidal group and dispersion mechanism of $In(OH)_3$ NPs prepared with CTAB as dispersant can be explained by Fig. 5. As an excellent cationic surfactant, CTAB is easily adsorbed onto negatively charged surface of $In(OH)_3$ powders. CTAB, also as a strong electrolyte, is dissociated completely when the $In(OH)_3$ NPs is dispersed into water. Due to the dissociation of CTAB, the surface charge of $In(OH)_3$ NPs changes from negative to positive. Meanwhile, the steric effect can further increase the dispersion of $In(OH)_3$ NPs on account of the long-chain of CTAB adsorbed on the surface.

Figure 6a shows the Zeta potential of $In(OH)_3$ NPs prepared with different concentrations of CTAB and the inserts are SEM images of the corresponding ITO NPs. As can be seen from Fig. 6a, the Zeta potential increases with the

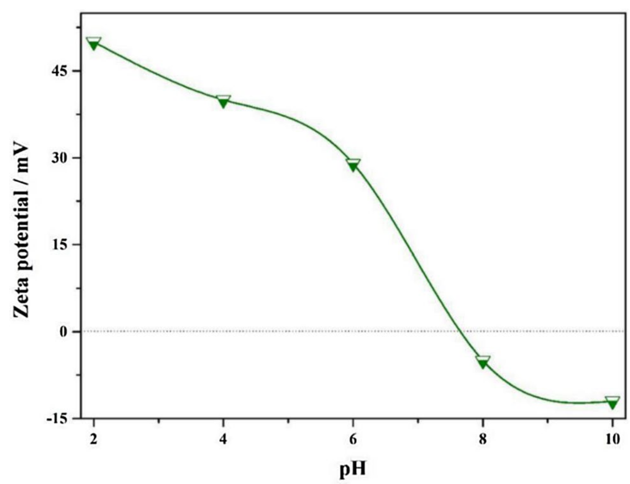

Fig. 4 Zeta potential of $In(OH)_3$ prepared at different pH values

increase of CTAB concentration. When the concentration of CTAB is added to 1.5 g/L, the Zeta potential almost no longer increase, indicating that the adsorption capacity of CTAB on the surface of $In(OH)_3$ NPs reaches to saturation. And the Zeta potential value of $In(OH)_3$ increases from −4.5 to 13.0 mV, indicating that the dispersion of $In(OH)_3$ NPs is promoted significantly. Meanwhile, the steric effect can also further increase the dispersion of $In(OH)_3$ NPs on account of the long-chain of CTAB adsorbed on the surface. Therefore, ITO NPs with high dispersibility can be prepared by dehydrated of the as-prepared $In(OH)_3$ NPs. And the inserted SEM images show the consistent results. In addition, Fig. 6b shows a narrow size distribution of ITO NPs obtained at the optimum addition amount of 1.5 g/L of CTAB, and the particle size ranges from 15 to 30 nm [35, 36].

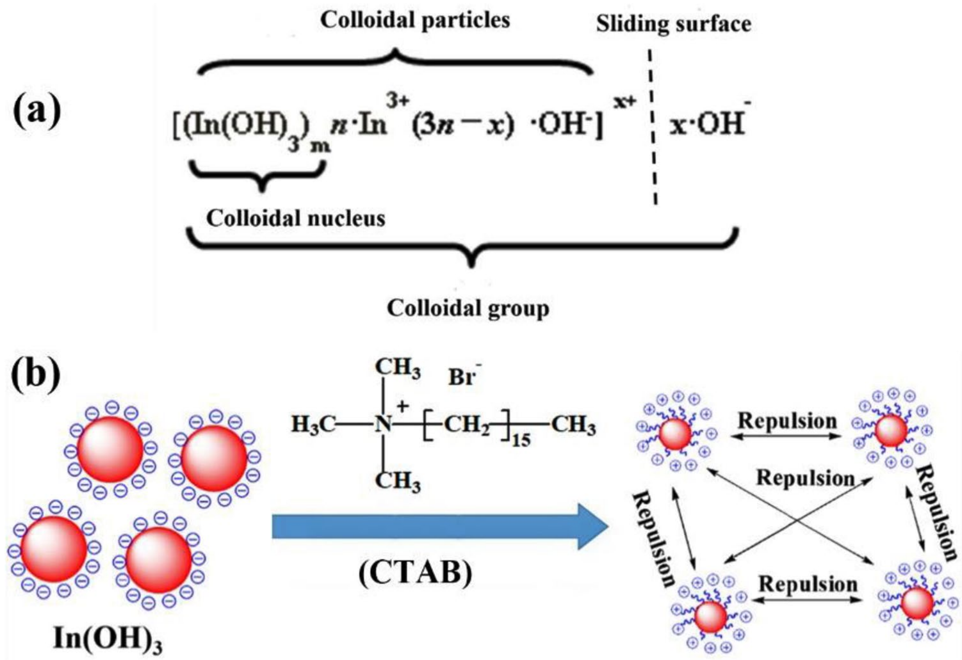

Fig. 5 **a** Structure of $In(OH)_3$ colloidal group and **b** dispersion mechanism of CTAB adsorbed on the surface of $In(OH)_3$ NPs

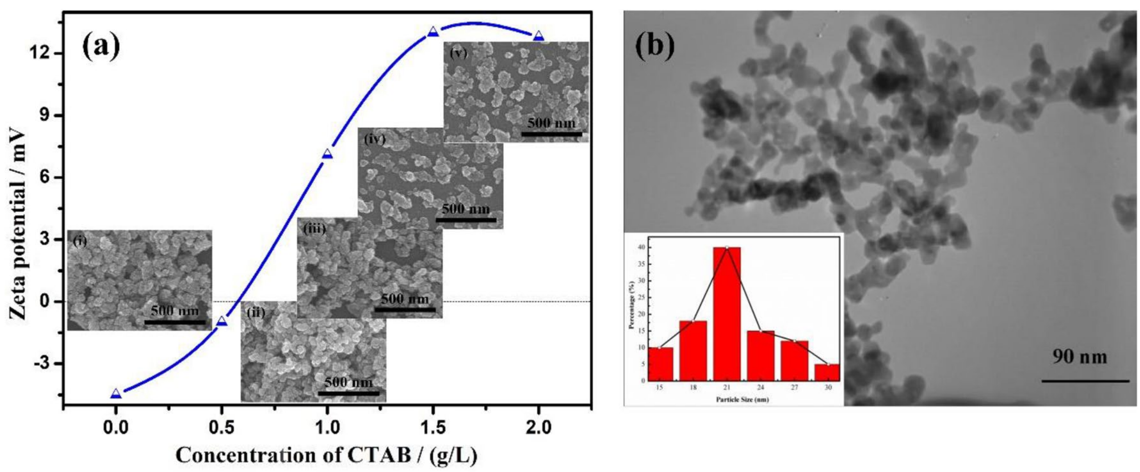

Fig. 6 **a** Zeta potential of $In(OH)_3$ and the inserted SEM images of corresponding ITO NPs prepared with different concentrations of CTAB: (i) 0.0 g/L, (ii) 0.5 g/L, (iii) 1.0 g/L, (iv) 1.5 g/L, (v) 2.0 g/L, **b** TEM image of ITO NPs prepared with 1.5 g/L of CTAB

3.3 The effects of dispersion on the light performance of ITO NPs

As one of important conductive substrates for photoelectric materials, ITO powders with high visible light transmittance and low resistivity are indispensable for preparing ITO conductive films of high quality [37]. Figure 7 shows the visible light transmittance spectra of ITO NPs prepared with different concentrations of CTAB. As shown in Fig. 7, the visible light transmittance of ITO NPs is increased from 70 to 92%, indicating the excellent effect of CTAB on improving the visible light transmittance of ITO NPs. It is obvious that the maximum visible light transmittance reaches 92% at the CTAB concentration of 1.5 g/L. This result can be explained via porosity which is a function of the refractive index shown in Eqs. (5–7) [38, 39].

$$n^2 = H + \sqrt{H^2 - n_0^2 n_s^2} \tag{5}$$

$$H = \frac{1}{2}\left(n_0^2 + n_s^2\right) + 2n_0 n_s \left[\frac{T_{\max} - T_{\min}}{T_{\max} T_{\min}}\right] \tag{6}$$

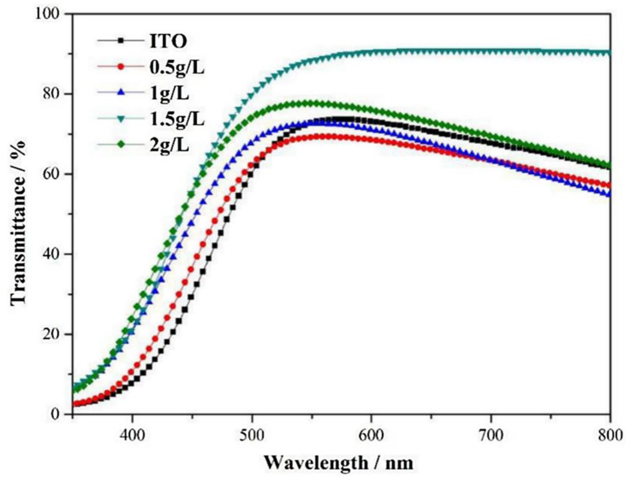

Fig. 7 Visible light transmittance spectra of ITO NPs prepared with different concentrations of CTAB

In this equation, n represents the refractive index, n_0 is the refractive index of air (1.00027), n_s is the refractive index of the substrate ($BaSO_4$) (1.636), T_{max} and T_{min} represent the upper and lower envelopes of the transmission spectrum, respectively.

$$\text{Porosity} = \left(1 - \frac{n^2 - 1}{n_d^2 - 1}\right)100\% \tag{7}$$

Wherein, n represents the refractive index, n_d is the refractive index of ITO NPs in a fully dense state (n_d=2.1).

Figure 8 shows the refractive spectra and porosity of ITO NPs prepared with different concentrations of CTAB. As shown in Fig. 8a, the refractive index decreases with the increase of wavelength, and this result was also obtained by Sasi et al. [40]. The calculation results of the porosity according to Eq. (7) are shown in Fig. 8b. In addition, Table 1 shows the effect of the absolute value of Zeta potential on the visible light transmittance of ITO NPs. As can be seen from Table 1, the ITO NPs with high absolute value of Zeta potential have a low porosity, showing small refractive index. The test results of the porosity of ITO NPs also show the same conclusion in Fig. 8b. Therefore, the visible light transmittance of ITO NPs was increased significantly. In other words, the dispersion of ITO NPs plays an important role in increasing the visible light transmittance. There is a favorable linear relationship between the visible light transmittance (T) of ITO NP and its absolute value of Zeta potential (μ), shown in Fig. 9. Equation (8) shows the corresponding fitting equation, and the correlation coefficient of 98.64% indicates highly linear relationship between the experimental data and the fitting line.

$$T = 60.862 + 2.287\mu\left(r^2 = 98.64\%\right) \tag{8}$$

Table 1 Effect of the absolute value of Zeta potential on the visible light transmittance of ITO NPs

Concentration (g/L)	Absolute value of Zeta potential (mV)	Min porosity (%)	Max transmittance (%)
0	4.5	46	70
0.5	1.0	48	65
1.0	7.1	42.5	75
1.5	13.0	32.5	92
2.0	12.8	37.5	78

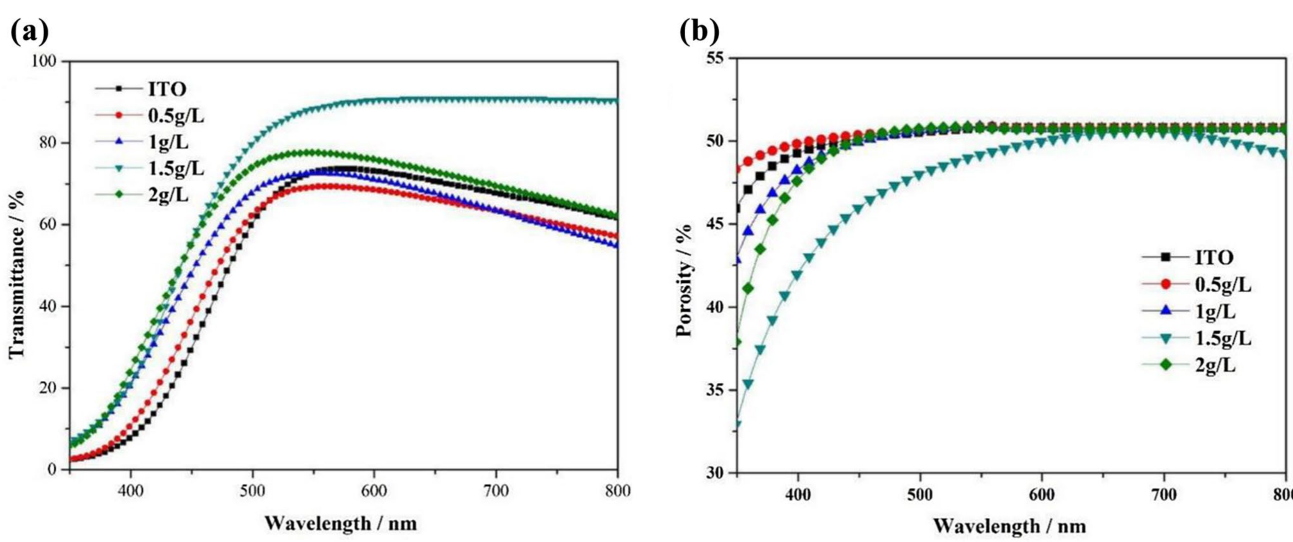

Fig. 8 **a** Refractive spectra and **b** porosity of ITO NPs prepared with different concentrations of CTAB

3.4 The effects of dispersion on the electrical performance of ITO NPs

Both optical and electrical properties are important for ITO films. Figure 10 shows the resistivity of ITO NPs prepared with different concentrations of CTAB. It is obvious that the concentration of CTAB plays a significant role in decreasing resistivity of ITO NPs, which can be confirmed by Fig. 10. In addition, the smaller the porosity, the lower the resistivity [41]. Due to the increase in the absolute value of Zeta potential, the porosity of ITO NPs decreased (Table 1), resulting in a lower resistivity of ITO NPs synthesized with 1.5 g/L of CTAB than that of ITO NPs prepared without CTAB assisted. With the increase of the concentration of CTAB, the absolute value of Zeta potential of ITO NPs increases significantly until the adsorption of CTAB on the surface of ITO NPs reaches saturation, which causes the resistivity of ITO NPs to decrease first and then remain stable. This result can also be obtained from Table 2. The minimum value of resistivity of 3.5×10^{-1} Ω cm is obtained under the condition that the absolute value of Zeta potential of ITO NPs is 13 mV. In addition, the linear fit between the resistivity of ITO NP and its absolute value of Zeta potential is shown in Fig. 11. Equation (9) is the corresponding fitting equation, and the correlation coefficient of 99.27% shows a favorable linear relationship between the absolute value of Zeta potential (μ) of ITO NP and its resistivity (ρ). In other words, the dispersion of ITO NPs plays an important role in decreasing their resistivity.

$$\rho = 0.7968 - 0.0350\mu\left(r^2 = 99.27\%\right) \tag{9}$$

Table 3 shows the summarization of resistivity of ITO NPs prepared via different methods. As can be seen from Table 3, the resistivity of ITO NPs synthesized by co-precipitation method is the lowest. And the resistivity of ITO NPs prepared without CTAB assisted in this paper is similar to those of Refs. [26] and [43]. However, the resistivity of ITO NPs prepared with 1.5 g/L of CTAB is significantly lower than those of Refs. [26] and [43]. Therefore, CTAB can significantly reduce the resistivity

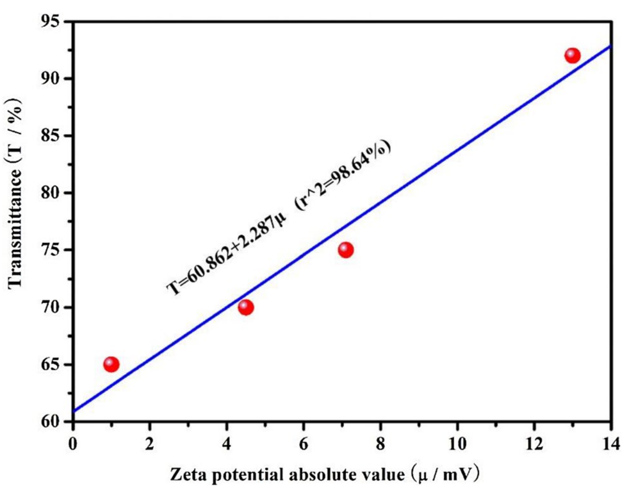

Fig. 9 Linear fit of the visible light transmittance of ITO NP and its absolute value of Zeta potential

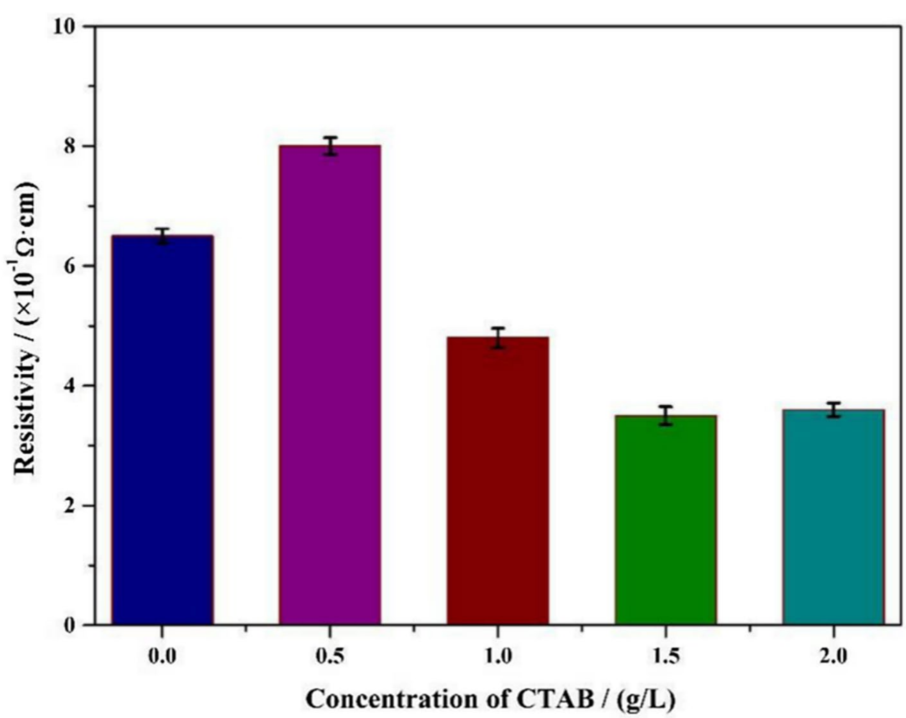

Fig. 10 Resistivity of ITO NPs prepared with different concentrations of CTAB

Table 2 Effect of the absolute value of Zeta potential on the resistivity

Number	Concentration (g/L)	Absolute value of Zeta potential (mV)	Resistivity (Ω cm)
1	0	4.5	0.64
2	0.5	1.0	0.78
3	1.0	7.1	0.51
4	1.5	13.0	0.35
5	2.0	12.8	0.36

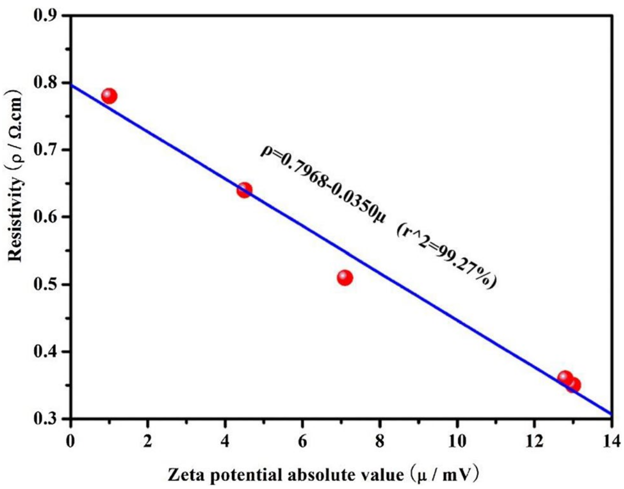

Fig. 11 Linear fit of the resistivity of ITO NP and its absolute value of Zeta potential

Table 3 Summarization of resistivity of ITO NPs prepared via different methods

References	Method	Resistivity of ITO NPs (Ω·cm)
[26]	Co-precipitation	0.64
[42]	Hydrothermal	1.25
[43]	Co-precipitation	4.90
[44]	Supercritical solvothermal	0.64
[45]	Co-precipitation	2.51
This paper	Co-precipitation (no CTAB)	0.65
	Co-precipitation (with CTAB)	0.35

of ITO NPs. In other words, the high dispersion of ITO NPs has a great contribution to decreasing its resistivity.

4 Conclusion

In this paper, a facile and effective method for decreasing the resistivity and increasing the visible light transmittance of ITO NPs was reported. CTAB as an excellent dispersant was used to improve the performance of ITO NPs synthesized by chemical coprecipitation method for the first time. When the concentration of CTAB was added to 1.5 g/L, the surface potential of ITO NPs was improved from − 4.5 to 13.0 mV, which caused a significant increase in visible light transmittance of ITO NPs from 70 to 92% and a remarkable decrease in resistivity from 6.5×10^{-1} to 3.5×10^{-1} Ω cm. The fitting equation between the visible light transmittance (T) of ITO NP and its absolute value of Zeta potential (μ) was $T = 60.862 + 2.287\mu$, while the fitting equation of its resistivity (ρ) and absolute value of Zeta potential (μ) was $\rho = 0.7968 - 0.0350\mu$. The correlation coefficients of the above two equations were 98.64% and 99.27%, respectively, indicating a highly linear relationship between the experimental data and the fitting line. This result showed that the excellent dispersion of ITO NPs had a great contribution to improving its optical and electric properties. In addition, the equation established based on the dispersion of ITO NPs in our paper can be used to forecast their optical and electric performance. And it is of important guiding significance and theoretical basis for domestic and foreign scholars to further improve the performance of ITO NPs. We believe that the optical and electric properties of ITO will be further increased via synthesizing ITO NPs with high dispersibility.

Acknowledgements This work was financially supported by Beijing Natural Science Foundation (No. 2192041).

Compliance with ethical standards

Conflicts of interest There are no conflicts of interest to declare.

References

1. G. Genesio, J. Maynadie, M. Carboni, D. Meyer, New J. Chem. **42**, 2351–2363 (2018)
2. S. Yang, J. Zhong, B. Sun, X. Zeng, W. Luo, X. Zhao, Y. Shu, J. Chen, J. He, J. Mater. Sci.: Mater. Electron. **30**, 13005–13012 (2019)
3. A. Murali, H.Y. Sohn, Mater. Res. Express **5**, 065045 (2018)
4. Y. Yan, Y. Wei, C. Zhao, M. Shi, L. Chen, C. Fan, M.J. Carnie, R. Yang, Y. Xu, J. Solid State Chem. **269**, 24–29 (2019)
5. Y. Shao, X. Xiao, L. Wang, Y. Liu, S. Zhang, Adv. Funct. Mater. **24**, 4170–4175 (2014)
6. A. Dolgonos, T.O. Mason, K.R. Poeppelmeier, J. Solid State Chem. **240**, 43–48 (2016)
7. Y. Luo, Y. Zhang, J. Huang, CrystEngComm **19**, 6972–6978 (2017)

8. C. Sun, C.H. Cheng, B.L. Zhang, R.X. Li, Y. Wang, W.F. Liu, Y.M. Luo, G.T. Du, S.L. Cong, Appl. Surf. Sci. **422**, 125–129 (2017)
9. E.B. Aydin, M.K. Sezginturk, Trac-Trends Anal. Chem. **97**, 309–315 (2017)
10. B.C. Yadav, K. Agrahari, S. Singh, T.P. Yadav, J. Mater. Sci.: Mater. Electron. **27**, 4172–4179 (2016)
11. O.V. Zhilova, S.Y. Pankov, A.V. Sitnikov, Y.E. Kalinin, M.N. Volochaev, V.A. Makagonov, J. Mater. Sci.: Mater. Electron. **30**, 11859–11867 (2019)
12. S.J. Shih, Y.C. Lin, S.H. Lin, P. Veteska, D. Galusek, W.H. Tuan, Ceram. Int. **42**, 11324–11329 (2016)
13. R.R. Kumar, K.N. Rao, K. Rajanna, A.R. Phani, Mater. Res. Bull. **52**, 167–176 (2014)
14. T. Ito, H. Uchiyama, H. Kozuka, Langmuir **33**, 5314–5320 (2017)
15. S. Khalid, E. Ahmed, M.A. Malik, D.J. Lewis, S.A. Bakar, Y. Khan, P. Brien, New J. Chem. **39**, 1013–1021 (2015)
16. C.J. Capozzi, R.A. Gerhardt, Adv. Funct. Mater. **17**, 2515–2521 (2007)
17. C. Kim, Y.H. Kim, Y.Y. Noh, S.J. Hong, M.J. Lee, Adv. Electron. Mater. **4**, 1700429 (2018)
18. A.H. Ali, A.S. Bakar, Z. Hassan, Appl. Surf. Sci. **315**, 387–391 (2014)
19. C. David, B.P. Tinkham, P. Prunici, A. Panckow, Surf. Coat. Technol. **314**, 113–117 (2016)
20. H. Zhang, C. Nie, J. Wang, R. Guan, D. Cao, Talanta **195**, 713–719 (2019)
21. E. Ye, S.Y. Zhang, S.H. Lim, S. Liu, M.Y. Han, Phys. Chem. Chem. Phys. **12**, 11923–11929 (2010)
22. X. Zhai, Y. Chen, Y. Ma, Y. Liu, J. Liu, Ceram. Int. (2019). https://doi.org/10.1016/j.ceramint.2019.05.319
23. S.C. Kulkarni, D.S. Patil, J. Mater. Sci.: Mater. Electron. **27**, 3731–3735 (2016)
24. Y. Yu, S. Qu, D. Zang, L. Wang, H. Wu, Nanoscale Res. Lett. **13**, 50 (2018)
25. G.G. Xu, X.D. Zhang, W. He, H. Liu, H. Li, R.I. Boughton, Mater. Lett. **60**, 962–965 (2006)
26. Y.Q. Zhang, J.X. Liu, Chin. J. Inorg. Chem. **33**, 249–254 (2017)
27. D. Lan, M. Qin, R. Yang, H. Wu, Z. Jia, K. Kou, G. Wu, Y. Fan, Q. Fu, F. Zhang, J. Mater. Sci.: Mater. Electron. **30**, 8771–8776 (2019)
28. T.I. Zubar, V.M. Fedosyuk, A.V. Trukhanov, N.N. Kovaleva, K.A. Astapovich, D.A. Vinnik, E.L. Trukhanova, A.L. Kozlovskiy, M.V. Zdorovets, A.A. Solobai, D.I. Tishkevich, S.V. Trukhanov, J. Electrochem. Soc. **166**, D173–D180 (2019)
29. Y. Masuda, T. Ohji, K. Kato, J. Solid State Chem. **189**, 21–24 (2012)
30. F. Mei, T. Yuan, R. Li, K. Qin, W. Zhao, S. Jiang, Ceram. Int. **44**, 7491–7499 (2018)
31. H. Wu, G. Wu, Y. Ren, X. Li, L. Wang, Chemistry A **22**, 8864–8871 (2016)
32. D. Selvakumar, N. Dharmaraj, K. Kadirvelu, N.S. Kumar, V.C. Padaki, Spectrochimica Acta Part A **133**, 335–339 (2014)
33. L.T. Lin, L. Tang, R. Zhang, C. Deng, D.J. Chen, L.W. Cao, J.-X. Meng, Mater. Res. Bull. **64**, 139–145 (2015)
34. Y. Liu, J. Liu, Mater. Res. Express **6** (2019)
35. B. Warcholinski, A. Gilewicz, T.A. Kuznetsova, T.I. Zubar, S.A. Chizhik, S.O. Abetkovskaia, V.A. Lapitskaya, Surf. Coat. Technol. **319**, 117–128 (2017)
36. Z. Chen, X. Qin, T. Zhou, X. Wu, S. Shao, M. Xie, Z. Cui, J. Mater. Chem. C **3**, 11464–11470 (2015)
37. J. Parra Barranco, F.J. Garcia Garcia, V. Rico, A. Borras, C. Lopez Santos, F. Frutos, A. Barranco, A.R. Gonzalez Elipe, Acs Appl. Mater. Interfaces **7**, 10993–11001 (2015)
38. H.N. Cui, V. Teixeira, A. Monteiro, Vacuum **67**, 589–594 (2002)
39. M. Gross, A. Winnacker, P.J. Wellmann, Thin Solid Films **515**, 8567–8572 (2007)
40. B. Sasi, K.G. Gopchandran, P.K. Manoj, P. Koshy, P. Prabhakara Rao, V.K. Vaidyan, Vacuum **68**, 149–154 (2002)
41. W.F. Cai, J.F. Geng, K.B. Pu, Q. Ma, D.W. Jing, Y.H. Wang, Q.Y. Chen, H. Liu, Chem. Eng. J. **333**, 572–582 (2018)
42. Y. Zhang, J. Liu, Chem. J. Chin. Univ. Chin. **38**, 1110–1116 (2017)
43. V. Senthilkumar, K. Senthil, P. Vickraman, Mater. Res. Bull. **47**, 1051–1056 (2012)
44. B. Shong, N. Shin, Y.H. Lee, K.H. Ahn, Y.W. Lee, J. Supercrit. Fluids **113**, 39–43 (2016)
45. X. Zhang, J. Liu, Rare Met. Mater. Eng. **46**, 1714–1718 (2017)